

Importance of exact exchange to the geometric and electronic structures of $\text{Cs}_2\text{BB}'\text{X}_6$ double perovskites

Yuyang Ji,[†] Peize Lin,^{*,¶} Xinguo Ren,^{*,¶} and Lixin He^{*,†}

[†]*Key Laboratory of Quantum Information, University of Science and Technology of China, Hefei, Anhui, 230026, People's Republic of China*

[‡]*Synergetic Innovation Center of Quantum Information and Quantum Physics, University of Science and Technology of China, Hefei, 230026, People's Republic of China*

[¶]*Songshan Lake Materials Laboratory, Dongguan 523808, Guangdong, China*

[§]*Institute of Physics, Chinese Academy of Sciences, Beijing 100190, China*

E-mail: linpeize@sslslab.org.cn; renxg@iphy.ac.cn; helx@ustc.edu.cn

Abstract

We investigate the lead-free halide double perovskites (HDPs) $\text{Cs}_2\text{BB}'\text{X}_6$ ($B=\text{Ag}, \text{Na}; B'=\text{In}, \text{Bi}; X=\text{Cl}, \text{Br}$) via first-principles calculations. We find that both the geometric and electric structures of the HDPs obtained by the Heyd-Scuseria-Ernzerhof (HSE) hybrid functional are much better than those of the Perdew-Burke-Ernzerhof (PBE) functional. Importantly, we find that the electronic structures of DHPs are very sensitive to their geometries, especially the B - X bond lengths. As a consequence, the electronic structures calculated by the HSE functional using the PBE optimized geometries may still significantly underestimate the band gaps, whereas the calculations on the HSE optimized geometries provide much more satisfactory results. The sensitivity of the band gaps of the DHPs to their geometries opens a promising path for the band

structure engineering via doping and alloying. This work therefore provides an useful guideline for further improvement of HDPs materials.

Hybrid perovskites (HPs) exhibit excellent transport and optical properties, such as high carrier mobility,¹ long carrier diffusion lengths²⁻⁵ and strong absorption coefficients.⁶ The power conversion efficiency (PCE) of HP solar cells has reached 29.5%.⁷ However, the limitation of toxicity and instability still need to be overcome for further improvement.

Lead-free halide double perovskites (HDPs) with formula $A_2BB'X_6$ have been proposed as environmentally friendly alternatives⁸⁻¹³ to HPs with long working lifetimes and have been applied in various optoelectronic devices, e.g. LEDs,^{9,12} photocatalysts¹⁴ and solar cells.¹⁵⁻¹⁸ For most HDPs, A is chosen as a Cs^+ or organic cation with a large ionic radius to stabilize the crystal structure, while X represents a halide ion. B and B' are occupied by monovalent and trivalent elements, respectively, such as Ag^+ , Na^+ and Bi^{3+} , In^{3+} . Compared to conventional HPs, most HDPs have large band gaps which limit their applications in the visible region. The band structures can be engineered by chemical substitution, alloying and doping strategies.^{9,10,12,13,19} Density functional theory (DFT) is a powerful tool to study the geometric and electronic structures of the materials, and therefore may provide useful guidance for the band structures engineering of DHPs.

In this work, we investigate five HDPs, including $\text{Cs}_2\text{AgInCl}_6$, $\text{Cs}_2\text{NaInCl}_6$, $\text{Cs}_2\text{AgBiCl}_6$, $\text{Cs}_2\text{AgBiBr}_6$ and $\text{Cs}_2\text{NaBiCl}_6$, via DFT calculations. We compare the results obtained by the Perdew-Burke-Ernzerhof (PBE) semilocal functional²⁰ and Heyd-Scuseria-Ernzerhof (HSE) hybrid functional.^{21,22} The results show that HSE can predict much better geometries of the DHPs, including the lattice constants and the B - X bond lengths. Importantly, we find that the electronic structures of DHPs are very sensitive to their geometries, especially the B - X bond lengths. As a consequence, the electronic structures calculated by the HSE functional using the PBE optimized structures may still significantly underestimate the band gaps, whereas the calculations based on the HSE optimized geometries can give much better results. The sensitivity of the band gaps of the DHPs to their geometries opens a promising

path for band structure engineering by doping and alloying.

The first-principles calculations are carried out using the Atomic-orbital Based Ab-initio Computation at USTC (ABACUS) package.^{23–25} We use both the PBE and HSE functionals in the calculations. In the HSE calculations, the mixing parameter of the Hartree-Fock exchange, $\alpha=0.25$ is used for DHPs with $B=\text{Na}$, and $\alpha=0.4$ is used for other DHPs, to obtain good agreement of the band gaps with the experiments. The spin-orbit coupling (SOC) effects are taken into account to calculate the band structures.

We adopt the SG15²⁶ optimized norm conserving Vanderbilt-type (ONCVP) pseudopotentials,²⁷ where Cs: $5s^25p^66s$, Ag: $4s^24p^64d^{10}5s$, In: $4d^{10}5s^25p$, Cl: $3s^23p^5$, Bi $5d^{10}6s^26p^3$ and Br: $4s^24p^5$ electrons are treated as valence electrons. The second generation NAO bases, namely the DPSI bases sets,²⁸ are used in all calculations. More specifically, Cs with $[4s\ 2p\ 1d]$, Ag with $[4s\ 2p\ 2d\ 1f]$, In with $[2s\ 2p\ 2d]$, Cl with $[2s\ 2p\ 1d]$, Na with $[4s\ 2p\ 1d]$, Bi with $[2s\ 2p\ 2d]$, Br with $[2s\ 2p\ 1d]$ NAOs are used. The $8\times8\times8$ Γ -centered Monkhorst-Pack \mathbf{k} -point mesh is used for the self-consistent calculations, and a $12\times12\times12$ \mathbf{k} -point mesh is used to calculate the projected density of states (PDOS).

Figure 1 depicts the crystal structure of $A_2BB'X_6$ HDPs, which have $\text{Fm}\bar{3}\text{m}$ space group symmetry. The B and B' ions are located alternately in the center of the AX_6 octahedra. The B - X (B' - X) bond length, i.e. the distance between B (B') and X in the same octahedral units is marked as d_{B-X} ($d_{B'-X}$).

In previous first-principles calculations, the electronic structures of the HDPs calculated by hybrid functionals (HSE and PBE0) are usually performed on the geometries obtained by the LDA/GGA functionals^{15,19,29,30} partly because the computational cost of HSE is very expensive. It has been shown that the electronic structures of DHP can be sensitive to their geometries.^{8,10,11} In this study, we would like to examine the effects of the HSE on the geometries of the DHPs, and consequently the impact on their electronic structures.

We first calculate the lattice constants of the five HDPs by the PBE and HSE functionals, and the results are compared with the experimental values in Table 1. The lattice constants

are fitted by the Birch-Murnaghan³¹ equation of state (EOS). The mean absolute errors (MAEs) of the lattice constants calculated from the PBE and HSE functionals, with respect to the experimental values, are 0.197 Å and 0.120 Å, respectively. As we see, the lattice constants obtained by HSE are in much better agreement with the experimental values than those by PBE. We also compare the equilibrium bond length d_{B-X}^0 calculated by the PBE and HSE functionals. In order to reduce the degrees of freedom in the comparisons and to compare with the experimental results, the lattice constants are fixed to the experimental values. We also fix the center of B and adjacent X atoms within the same octahedra, and then move the two atoms to change the distance between them and obtain a series of geometries. During the movement, the distance between B and B' is fixed, which means that the length increased by d_{B-X} is equal to the length reduced by $d_{B'-X}$, thus, the symmetry is maintained. We estimate equilibrium bond lengths according to energy-versus-distance $[E(d)]$ curves of five solids by using two functionals. An example of $E(d)$ can be found in the supplemental materials. The results are listed in Table 2, and compared with the experimental values. The PBE significantly underestimates the $B-X$ bond lengths, whereas HSE yields much better $B-X$ bond lengths with a MAE of 0.008 Å, which is significantly less than the MAE of the PBE functional 0.038 Å.

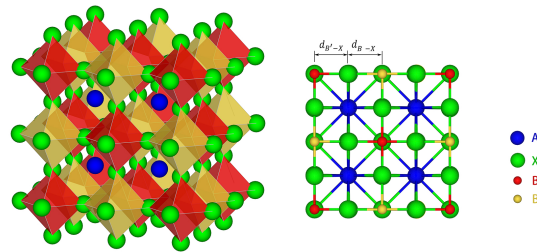


Figure 1: Crystal structure of $A_2BB'X_6$ with bond lengths d_{B-X} and $d_{B'-X}$.

Table 1: HSE lattice constants (in Å) were fitted by Birch-Murnaghan³¹ equation of state (EOS).

	PBE	HSE	Experiment
Cs ₂ AgInCl ₆	10.678	10.564	10.481 ⁸
Cs ₂ NaInCl ₆	10.711	10.599	10.514, ³² 10.534 ¹⁰
Cs ₂ AgBiCl ₆	10.974	10.946	10.777 ^{19,33}
Cs ₂ AgBiBr ₆	11.447	11.380	11.250 ³⁴
Cs ₂ NaBiCl ₆	11.036	10.966	10.839, ³⁵ 10.842 ¹⁰
MAE	0.197	0.120	

Table 2: Comparison of the equilibrium bond lengths d_{B-X}^0 (in Å) obtained by PBE and HSE functionals with the experimental values.

	PBE	HSE	Experiment
Cs ₂ AgInCl ₆	2.683	2.728	2.733 ⁸
Cs ₂ NaInCl ₆	2.721	2.743	2.748, ³² 2.763 ¹⁰
Cs ₂ AgBiCl ₆	2.670	2.698	2.707 ^{19,33}
Cs ₂ AgBiBr ₆	2.775	2.797	2.803 ³⁴
Cs ₂ NaBiCl ₆	2.703	2.736	2.754 ^{10,35}
MAE	0.038	0.008	

To see how the crystal structures affect the electronic structures in the DHP materials, we calculate the band gaps as functions of the $B-X$ bond lengths.

Figure 2(a) depicts the band gaps as functions of Ag-Cl bond length calculated by PBE and HSE functionals for Cs₂AgInCl₆. The experimental lattice constant is used. Cs₂AgInCl₆ shows a negligible SOC effect in our calculations, and therefore, we show only the results without SOC. As we see from the figure, the HSE calculated band gap increases notably with increasing of Ag-Cl bond length, $d_{\text{Ag-Cl}}$. Even though the PBE functional significantly underestimates the gap, it predicts the similar trends of the band gaps changing with Ag-Cl bond length. The band gap calculated by HSE at the PBE Ag-Cl bond length (2.683 Å) is approximately 2.644 eV, which is significantly lower than the experimental value (3.3 eV), marked by the red triangle in the figure. In contrast, the band gap calculated at the HSE optimized Ag-Cl bond length (2.728 Å) is approximately 3.047 eV, which is in excellent agreement with the experimental value. These results suggest that the band gap

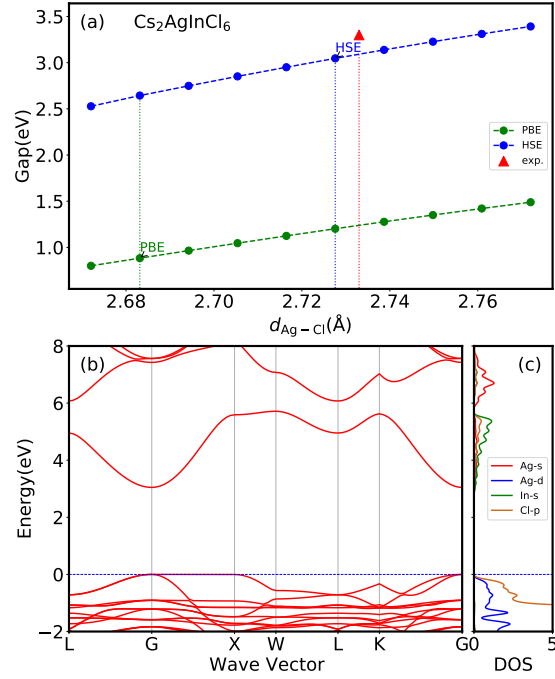


Figure 2: (a) Band gaps of $\text{Cs}_2\text{AgInCl}_6$ with a lattice constant of 10.481 \AA predicted by PBE and HSE as a function of bond length $d_{\text{Ag-Cl}}$. The experimental structure and band gap were obtained from Ref. 8. (b)-(c) Band structure and partial DOS of $\text{Cs}_2\text{AgInCl}_6$ with $d_{\text{Ag-Cl}}^{0,\text{HSE}}$ calculated using the HSE functional.

calculated by HSE on the geometry obtained by the PBE functional would still significantly underestimate the band gap.

Figure 2(b) shows the band structure of $\text{Cs}_2\text{AgInCl}_6$ calculated by the HSE functional, using the $d_{\text{Ag-Cl}}$ also obtained by the HSE. The corresponding PDOS are shown in Fig. 2(c). The lowest conduction band (CB) of $\text{Cs}_2\text{AgInCl}_6$ is very dispersive, since it is dominated by the delocalized Cl 3*p* and In 5*s* electrons with some small contribution from the Ag 5*s* states. The dispersive bands suggest that the electrons have very small effective masses, and therefore large carrier mobility, which is good for photoelectric device applications. The highest VB is much flatter, especially there is a flat band between the Γ and X points. This flat band originates from the hybridization of Cl 3*p*, and Ag 4*d* electrons [Fig. 2(c)] near the Fermi level .

We also calculate the band gaps as a function of Na-Cl bond length for $\text{Cs}_2\text{NaInCl}_6$ using standard HSE with mixing parameter of 0.25, and find that the trend of band gaps over the Na-Cl bond length is very similar to that of $\text{Cs}_2\text{AgInCl}_6$. More results of the electronic structures for $\text{Cs}_2\text{NaInCl}_6$ can be found in the supplemental materials.

Substituting In with Bi in $\text{Cs}_2\text{AgInCl}_6$ would be expected to result in very different band structures. $\text{Cs}_2\text{AgBiCl}_6$ has a much larger lattice constant of 10.777 Å than $\text{Cs}_2\text{AgInCl}_6$, and the Bi ion introduces strong SOC effects. Indeed, $\text{Cs}_2\text{AgBiCl}_6$ has an indirect band gap, in contrast to $\text{Cs}_2\text{AgInCl}_6$. The feature of the indirect band gap of this compound is captured by both PBE and HSE functionals, with or without SOC. We plot the (indirect) band gaps as functions of Ag-Cl bond length for both PBE and HSE functionals. Similar to the case of $\text{Cs}_2\text{AgInCl}_6$, both PBE and HSE functionals predict that the band gap increases with increasing $d_{\text{Ag-Cl}}$ for $\text{Cs}_2\text{AgBiCl}_6$, although the magnitude is less dramatic, as shown in Fig. 3(a). The PBE calculated band gap at the HSE calculated Ag-Cl bond length, is 1.807 eV without SOC, and decreases to 1.547 eV after turning on SOC, both significantly underestimate the experimental band gap of 2.77 eV. The band gap calculated by the HSE functional with nonstandard mixing parameter of 0.4 at this bond length is approximately

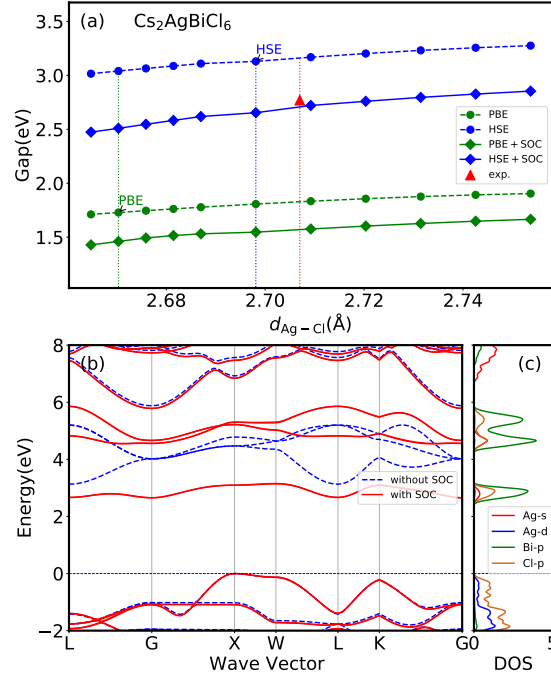


Figure 3: (a) Band gaps of $\text{Cs}_2\text{AgBiCl}_6$ with a lattice constant of 10.777 \AA predicted by four methods (i.e. PBE, PBE+SOC, HSE and HSE+SOC) as a function of bond length $d_{\text{Ag-Cl}}$. The experimental structure and band gap were obtained from Ref. 33. (b)-(c) Band structure and partial DOS with SOC of $\text{Cs}_2\text{AgBiCl}_6$ with $d_{\text{Ag-Cl}}^{0,\text{HSE}}$ calculated using the HSE+SOC functionals.

3.130 eV without SOC, which significantly overestimates the experimental band gap. After turning on the SOC, the band gap decreases by approximately 0.5 eV, and is in excellent agreement with the experimental gap marked as the red triangle in the figure. However, if we calculate the band gap using the PBE optimized Ag-Cl bond length, the band gap would be 0.145 eV smaller.

The band structures of $\text{Cs}_2\text{AgBiCl}_6$ are shown in Fig. 3(b). The band structures are calculated by HSE, with (red solid lines) and without (blue dashed lines) SOC. The experimental lattice constant is used, and the Ag-Cl bond length is determined from the HSE calculations. As shown in the figure, the strong SOC of the Bi atoms leads to giant splitting of the conduction bands, which significantly reduces the band gap. The direct band gap near the X point is approximately 3.092 eV, which is also in good agreement with the experimental value of 3.3 eV.¹⁹

Notably, the lowest CBs become much less dispersive compared to those without turning on SOC. Especially, the lowest CB becomes very flat after turning on SOC. This is different from the Pb-based perovskites, where SOC actually reduces the electron effective masses. PDOS [see Fig. 3(c)] analysis shows that the lowest conduction bands are made up mainly of Bi-6*p* states hybridized with Ag-5*s* and Cl-3*p* states, which split into two distinct peaks in PDOS under SOC. Shi and Du suggested that the flat CB in the Bismuth DHPs is due to the large electronegativity difference among cations and the large nearest-neighbor distances in cation sublattices.³⁶ Savory et al. argued that the flat CB band is due to a mismatch in angular momentum of the frontier atomic orbitals of the *B* and *B'* ions.²⁹ Here we show that the SOC also plays a crucial role for the flat CB bands in the Bismuth DHPs.

The band structures of $\text{Cs}_2\text{NaBiCl}_6$ and $\text{Cs}_2\text{AgBiBr}_6$ have very similar features to those of $\text{Cs}_2\text{AgBiCl}_6$. Detailed results for the two materials are given in the Supplementary Materials.

We investigate the geometries and electronic structures of $\text{Cs}_2\text{BB}'\text{X}_6$ DHPs via first-principles calculations. We compare the results given by the PBE and HSE functionals. The results show that HSE can predict much better geometries of the DHPs, including the lattice

constants and the $B-X$ bond lengths. Importantly, the electronic structures of DHPs are very sensitive to their geometries, especially the $B-X$ bond lengths. Therefore the electronic structures calculated by the HSE functional using the PBE optimized structures may still significantly underestimate the band gaps, whereas the calculations on the HSE optimized geometries can give much better results. The results indicate that mitigating the strong self-interaction errors are crucial for correctly describing not only the electronic structure, but also the geometries of DHP materials. The sensitivity of band gaps of the DHPs to their geometries opens a promising path for band structure engineering by doping and alloying.

Acknowledgement

This work was funded by the Chinese National Science Foundation Grant Numbers 12134012, 11874335, and 12188101. The numerical calculations were performed on the USTC HPC facilities.

Supporting Information Available

The following files are available free of charge.

- sm.pdf: Supplementary results for the paper.

References

- (1) Oga, H.; Saeki, A.; Ogomi, Y.; Hayase, S.; Seki, S. Improved Understanding of the Electronic and Energetic Landscapes of Perovskite Solar Cells: High Local Charge Carrier Mobility, Reduced Recombination, and Extremely Shallow Traps. *J. Am. Chem. Soc.* **2014**, *136*, 13818–13825.
- (2) Stranks, S. D.; Eperon, G. E.; Grancini, G.; Menelaou, C.; Alcocer, M. J. P.; Lei-

- jens, T.; Herz, L. M.; Petrozza, A.; Snaith, H. J. Electron-Hole Diffusion Lengths Exceeding 1 Micrometer in an Organometal Trihalide Perovskite Absorber. *Science* **2013**, *342*, 341–344.
- (3) Xing, G.; Mathews, N.; Sun, S.; Lim, S. S.; Lam, Y. M.; Grätzel, M.; Mhaisalkar, S.; Sum, T. C. Long-Range Balanced Electron- and Hole-Transport Lengths in Organic-Inorganic $\text{CH}_3\text{NH}_3\text{PbI}_3$. *Science* **2013**, *342*, 344–347.
- (4) Dong, Q.; Fang, Y.; Shao, Y.; Mulligan, P.; Qiu, J.; Cao, L.; Huang, J. Electron-hole diffusion lengths $> 175 \mu\text{m}$ in solution-grown $\text{CH}_3\text{NH}_3\text{PbI}_3$ single crystals. *Science* **2015**, *347*, 967–970.
- (5) Shi, D.; Adinolfi, V.; Comin, R.; Yuan, M.; Alarousu, E.; Buin, A.; Chen, Y.; Hoogland, S.; Rothenberger, A.; Katsiev, K., et al. Low trap-state density and long carrier diffusion in organolead trihalide perovskite single crystals. *Science* **2015**, *347*, 519–522.
- (6) De Wolf, S.; Holovsky, J.; Moon, S.-J.; Löper, P.; Niesen, B.; Ledinsky, M.; Haug, F.-J.; Yum, J.-H.; Ballif, C. Organometallic Halide Perovskites: Sharp Optical Absorption Edge and Its Relation to Photovoltaic Performance. *J. Phys. Chem. Lett.* **2014**, *5*, 1035–1039.
- (7) NREL, Best Research-Cell Efficiencies chart. <https://www.nrel.gov/pv/assets/pdfs/best-research-cell-efficiencies-rev211117.pdf>.
- (8) Volonakis, G.; Haghighirad, A. A.; Milot, R. L.; Sio, W. H.; Filip, M. R.; Wenger, B.; Johnston, M. B.; Herz, L. M.; Snaith, H. J.; Giustino, F. $\text{Cs}_2\text{InAgCl}_6$: A New Lead-Free Halide Double Perovskite with Direct Band Gap. *J. Phys. Chem. Lett.* **2017**, *8*, 772–778.
- (9) Luo, J.; Wang, X.; Li, S.; Liu, J.; Guo, Y.; Niu, G.; Yao, L.; Fu, Y.; Gao, L.; Dong, Q., et al. Efficient and stable emission of warm-white light from lead-free halide double perovskites. *Nature* **2018**, *563*, 541–545.

- (10) Zhou, J.; Rong, X.; Zhang, P.; Molokeev, M. S.; Wei, P.; Liu, Q.; Zhang, X.; Xia, Z. Manipulation of $\text{Bi}^{3+}/\text{In}^{3+}$ transmutation and Mn^{2+} -doping effect on the structure and optical properties of double perovskite $\text{Cs}_2\text{NaBi}_{1-x}\text{In}_x\text{Cl}_6$. *Adv. Opt. Mater.* **2019**, *7*, 1801435.
- (11) Ning, W.; Zhao, X.-G.; Klarbring, J.; Bai, S.; Ji, F.; Wang, F.; Simak, S. I.; Tao, Y.; Ren, X.-M.; Zhang, L.; Huang, W.; Abrikosov, I. A.; Gao, F. Thermochromic Lead-Free Halide Double Perovskites. *Adv. Funct. Mater.* **2019**, *29*, 1807375.
- (12) Majher, J. D.; Gray, M. B.; Strom, T. A.; Woodward, P. M. $\text{Cs}_2\text{NaBiCl}_6\text{:Mn}^{2+}$ —A New Orange-Red Halide Double Perovskite Phosphor. *Chem. Mater.* **2019**, *31*, 1738–1744.
- (13) Bartel, C. J.; Clary, J. M.; Sutton, C.; Vigil-Fowler, D.; Goldsmith, B. R.; Holder, A. M.; Musgrave, C. B. Inorganic Halide Double Perovskites with Optoelectronic Properties Modulated by Sublattice Mixing. *J. Am. Chem. Soc.* **2020**, *142*, 5135–5145.
- (14) Zhou, L.; Xu, Y.-F.; Chen, B.-X.; Kuang, D.-B.; Su, C.-Y. Synthesis and Photocatalytic Application of Stable Lead-Free $\text{Cs}_2\text{AgBiBr}_6$ Perovskite Nanocrystals. *Small* **2018**, *14*, 1703762.
- (15) Zhao, X.-G.; Yang, D.; Sun, Y.; Li, T.; Zhang, L.; Yu, L.; Zunger, A. Cu–In Halide Perovskite Solar Absorbers. *J. Am. Chem. Soc.* **2017**, *139*, 6718–6725.
- (16) Greul, E.; Petrus, M.; Binek, A.; Docampo, P.; Bein, T. Highly stable, phase pure $\text{Cs}_2\text{AgBiBr}_6$ double perovskite thin films for optoelectronic applications. *J. Mater. Chem. A* **2017**, *5*, 19972–19981.
- (17) Gao, W.; Ran, C.; Xi, J.; Jiao, B.; Zhang, W.; Wu, M.; Hou, X.; Wu, Z. High-Quality $\text{Cs}_2\text{AgBiBr}_6$ Double Perovskite Film for Lead-Free Inverted Planar Heterojunction Solar Cells with 2.2% Efficiency. *Chem. Phys. Chem.* **2018**, *19*, 1696–1700.

- (18) Pantaler, M.; Cho, K. T.; Queloz, V. I. E.; García Benito, I.; Fettinghauer, C.; Anusca, I.; Nazeeruddin, M. K.; Lupascu, D. C.; Grancini, G. Hysteresis-Free Lead-Free Double-Perovskite Solar Cells by Interface Engineering. *ACS Energy Lett.* **2018**, *3*, 1781–1786.
- (19) Volonakis, G.; Filip, M. R.; Haghighirad, A. A.; Sakai, N.; Wenger, B.; Snaith, H. J.; Giustino, F. Lead-Free Halide Double Perovskites via Heterovalent Substitution of Noble Metals. *J. Phys. Chem. Lett.* **2016**, *7*, 1254–1259.
- (20) Perdew, J. P.; Burke, K.; Ernzerhof, M. Generalized Gradient Approximation Made Simple. *Phys. Rev. Lett.* **1996**, *77*, 3865–3868.
- (21) Heyd, J.; Scuseria, G. E.; Ernzerhof, M. Hybrid functionals based on a screened Coulomb potential. *J. Chem. Phys.* **2003**, *118*, 8207–8215.
- (22) Krukau, A. V.; Vydrov, O. A.; Izmaylov, A. F.; Scuseria, G. E. Influence of the exchange screening parameter on the performance of screened hybrid functionals. *J. Chem. Phys.* **2006**, *125*, 224106.
- (23) Chen, M.; Guo, G.; He, L. Systematically improvable optimized atomic basis sets for ab initio calculations. *J. Phys. Condens. Matter* **2010**, *22*, 445501.
- (24) Li, P.; Liu, X.; Chen, M.; Lin, P.; Ren, X.; Lin, L.; Yang, C.; He, L. Large-scale ab initio simulations based on systematically improvable atomic basis. *Comput. Mater. Sci.* **2016**, *112*, 503–517.
- (25) <http://abacus.ustc.edu.cn> .
- (26) Schlipf, M.; Gygi, F. Optimization algorithm for the generation of ONCV pseudopotentials. *Comput. Phys. Commun.* **2015**, *196*, 36–44.
- (27) Hamann, D. R. Optimized norm-conserving Vanderbilt pseudopotentials. *Phys. Rev. B* **2013**, *88*, 085117.

- (28) Lin, P.; Ren, X.; He, L. Strategy for constructing compact numerical atomic orbital basis sets by incorporating the gradients of reference wavefunctions. *Phys. Rev. B* **2021**, *103*, 235131.
- (29) Savory, C. N.; Walsh, A.; Scanlon, D. O. Can Pb-Free Halide Double Perovskites Support High-Efficiency Solar Cells? *ACS Energy Lett.* **2016**, *1*, 949–955.
- (30) Zhou, J.; Xia, Z.; Molochev, M. S.; Zhang, X.; Peng, D.; Liu, Q. Composition design, optical gap and stability investigations of lead-free halide double perovskite Cs₂AgInCl₆. *J. Mater. Chem. A* **2017**, *5*, 15031–15037.
- (31) Birch, F. Finite Elastic Strain of Cubic Crystals. *Phys. Rev.* **1947**, *71*, 809–824.
- (32) Noculak, A.; Morad, V.; McCall, K. M.; Yakunin, S.; Shynkarenko, Y.; Wörle, M.; Kovalenko, M. V. Bright Blue and Green Luminescence of Sb(III) in Double Perovskite Cs₂MInCl₆ (M = Na, K) Matrices. *Chem. Mater.* **2020**, *32*, 5118–5124.
- (33) McClure, E. T.; Ball, M. R.; Windl, W.; Woodward, P. M. Cs₂AgBiX₆ (X = Br, Cl): New Visible Light Absorbing, Lead-Free Halide Perovskite Semiconductors. *Chem. Mater.* **2016**, *28*, 1348–1354.
- (34) Slavney, A. H.; Hu, T.; Lindenberg, A. M.; Karunadasa, H. I. A Bismuth-Halide Double Perovskite with Long Carrier Recombination Lifetime for Photovoltaic Applications. *J. Am. Chem. Soc.* **2016**, *138*, 2138–2141.
- (35) Morris, L.; Robinson, W. Crystal structure of Cs₂NaBiCl₆. *Acta Cryst. B* **1972**, *28*, 653–654.
- (36) Shi, H.; Du, M.-H. Discrete Electronic Bands in Semiconductors and Insulators: Potential High-Light-Yield Scintillators. *Phys. Rev. Applied* **2015**, *3*, 054005.